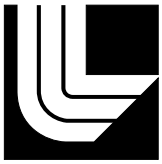

LAWRENCE
LIVERMORE
NATIONAL
LABORATORY

UCRL-TR-227505

Electrostatic Modeling of Vacuum Insulator Triple Junctions

L. K. Tully, D. A. Goerz, T. L. Houck, J. B. Javedani

October 25, 2006

This work was performed under the auspices of the U.S. Department of Energy by University of California, Lawrence Livermore National Laboratory under Contract W-7405-Eng-48.

ELECTROSTATIC MODELING OF VACUUM INSULATOR TRIPLE JUNCTIONS

L.K. Tully, D.A. Goerz, T.L. Houck, J.B. Javedani

ABSTRACT

Triple junctions are often initiation points for insulator flashover in pulsed power devices. The two-dimensional finite-element TriComp [1] modeling software suite was utilized for its electrostatic field modeling package to investigate electric field behavior in the anode and cathode triple junctions of a high voltage vacuum-insulator interface. TriComp enables simple extraction of values from a macroscopic solution for use as boundary conditions in a subset solution. Electric fields computed with this zoom capability correlate with theoretical analysis of the anode and cathode triple junctions within submicron distances for nominal electrode spacing of 1.0 cm. This paper will discuss the iterative zoom process with TriComp finite-element software and the corresponding theoretical verification of the results.

I. INTRODUCTION

Vacuum insulators are critical components in high energy pulsed power devices. The triple junction of vacuum, dielectric, and metal creates a unique environment for field enhancement and attendant possibility for breakdown or flashover. Accurate field modeling of triple junctions facilitates insulator design with higher voltage standoff capabilities.

For efficient use of computer memory, the mesh generators in many commercial finite-element modeling codes generate a "variable mesh". The variable mesh introduces large mesh sizes covering areas which the algorithm determines are regions of less field variability and thus of less interest. Increasingly smaller mesh sizes are formed as the solution area geometry increases in complexity. For example, sharp points or changes in dielectric materials trigger the mesh generator to reduce the mesh size in those areas. In contrast, the TriComp mesh generator (Mesh 5.0) builds a conformal mesh based on the user's mesh specifications. Mesh grid size can be adjusted in the x-y (or r-z) direction, but not adaptively in areas of interest as shown in Figure 1.

A limitation of the TriComp method is the inability to build small details in a comparatively large solution space. For instance, the mesh generator will fail to mesh a submicron needle in an area requiring a 10 μm mesh due to the large scale of the solution area. Conversely, an advantage of the TriComp method is the ability to easily include boundary conditions from previous solutions. This is achieved by assigning boundaries with potential values interpolated from a macroscopic (or global) solution.

Detailed views of electric field behavior can be achieved by repeatedly extracting values from a larger solution for use as boundary conditions in a subsection of that solution. This "iterative zooming" feature can be used to include small details after a global solution has been established. The zooming feature can also be utilized to study areas of interest such as the anode and cathode triple junctions in extreme detail.

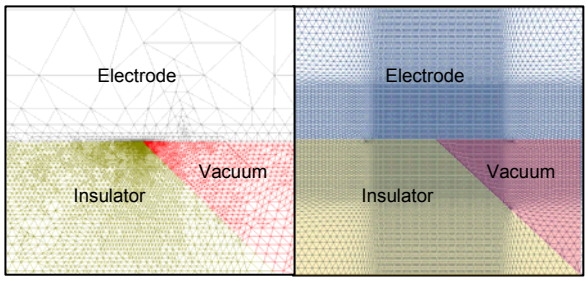

Figure 1. The mesh on the left is a variable conformal mesh. The mesh on the right was constructed by TriComp Mesh 5.0.

II. MODEL

The two-dimensional geometry modeled with TriComp consists of a disk-shaped anode and cathode with a truncated 45° cone insulator as shown in Figure 2. The insulator is 1 cm in height and is positioned between the anode and cathode. This entire configuration is placed inside a vacuum chamber with walls at ground potential. The anode is charged to positive 100 kV while the cathode also remains at ground potential.

Although the geometry of the device is rotationally symmetric about the r = 0 axis, the zooming procedure required the use of x-y coordinates with shift invariance in the z direction. The use of rectangular coordinates for this application is acceptable since the region of interest around the triple junction (submicron range) is significantly smaller than the curvature of the insulator itself. For best results, the coordinate system origin was placed at or very near the region of interest. Since the goal of the analysis was to study the anode and cathode triple junctions, mesh geometry was constructed with the origin located at either the anode triple junction (ATJ) or the cathode

triple junction (CTJ), respectively. This placement is recommended to avoid computational rounding errors in the representation of larger numbers separated by small increments. (Example: 15000.1 and 15000.2) The ability to work in such small fractions is invaluable in submicron electric field studies embedded in a relatively large solution space.

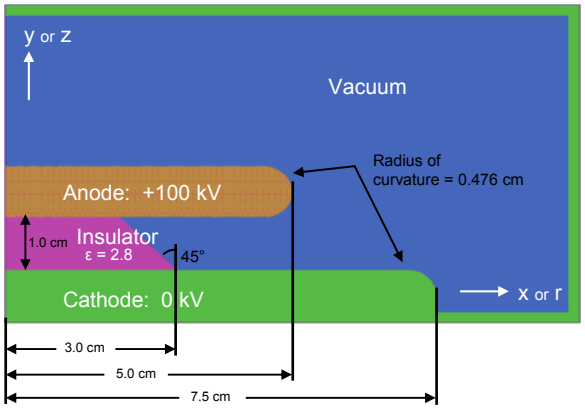

Figure 2. Global geometry: 6.0 cm x 10.0 cm

In the initial global geometry, as shown in Figure 2, the anode and cathode were assigned fixed potential Dirichlet boundaries of 100 kV and 0 kV respectively. The 45° insulator region was assigned a dielectric constant of 2.8. The initial mesh was constructed with a 30 μm mesh in the regions of interest including the anode, cathode, and insulator. The outermost areas were constructed with a 50 μm mesh.

The potential lines and electric field magnitude of the entire region are seen in Figure 3. Potential values along the boundaries were extracted and interpolated by the code from calculated values along those same lines in the previous solution. "Zoom" levels were constructed with mesh sizes of 10, 5, 1, and 0.2 μm as the solution region was significantly reduced at each step.

Additionally, new features such as rounded tips or small cracks can be added with the use of old boundaries as long as the added features are located a reasonable distance away from the boundaries themselves [2]. This was not necessary in the baseline case investigation of the ATJ and CTJ, but it proves valuable during studies of imperfections in the triple junctions.

Line scans were taken from the solution on both the vacuum and insulator sides of the interface as seen in Figure 4. The lines were one mesh size away from the insulator-vacuum interface and electrode surface. The results from these line scans are plotted in Figure 5. As expected, the tangential component of the electric field is the same on both the insulator and vacuum sides of the interface. The normal fields differ by a scale factor of the dielectric constant.

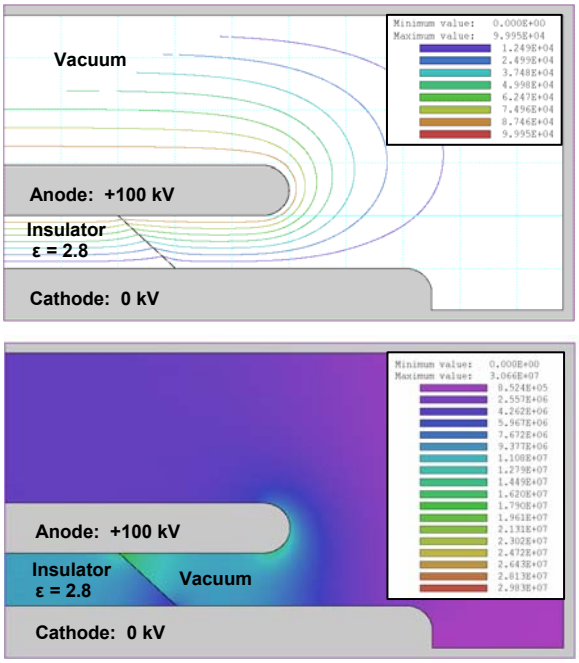

Figure 3. Potential and electric field results in global solution

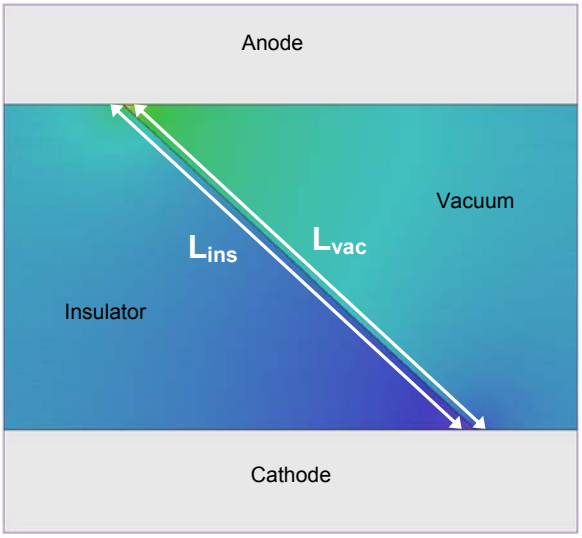

Figure 4. Definition of line scans taken along vacuum-insulator interface (shown on 10 μm mesh)

The maximum and minimum values in Table 1 are taken approximately one mesh size away from the triple junction. With each mesh size decrease (or zoom increase) it can be noted that the electric fields increase at the ATJ and decrease at the CTJ. It can be shown theoretically through the work of Takuma and Chung that the classical theoretical value of the electric field approaches infinity at the anode triple junction and

approaches zero at the cathode triple junction [3],[4],[5],[6],[7]. A summary of their approaches is given in the next section.

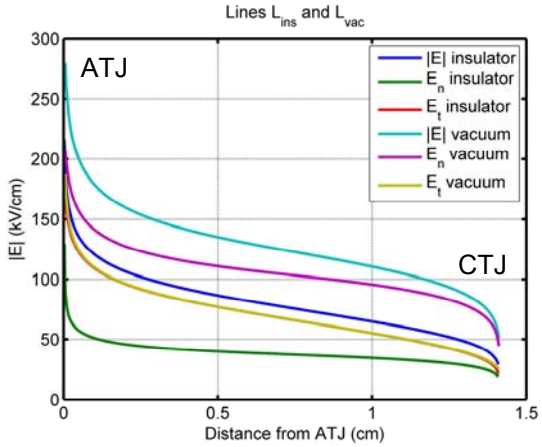

Figure 5. Line scan from ATJ to CTJ

Table 1. Increasing/decreasing electric field strength at ATJ/CTJ with decrease in mesh size

Mesh size (μm)	Max |E| field at ATJ (kV/cm)	Min |E| field at CTJ (kV/cm)
30	302	47
10	331	39
5	391	35
1	499	27
0.2	638	21

III. THEORY

Chung et al. describes the field behavior in the vacuum near the triple junction (for small r) as

$$E = Cr^{\nu-1} \quad \textbf{(1)}$$

where $C = A\nu$ and is independent of r and ϕ [5],[6],[7]. The transcendental equation

$$\varepsilon \tan(\nu\theta) = \tan(\pi - \nu\beta) \quad \textbf{(2)}$$

determines the value of ν based upon the angles described in Figure 6 and the dielectric constant ε.

Therefore, for the modeled 45° insulator case, the value of ν at the ATJ is 0.84778 and ν at the CTJ is 1.15222. From Eq. (1), the electric field at the ATJ and CTJ are written as

$$E_{ATJ} = Cr^{-0.15222} \quad \textbf{(3)}$$

$$E_{CTJ} = Cr^{+0.15222}. \quad \textbf{(4)}$$

As $r \to 0$,

$$E_{ATJ} \to \infty \quad \textbf{(5)}$$

$$E_{CTJ} \to 0. \quad \textbf{(6)}$$

In the dielectric, the electric field maintains the characteristics of approaching infinity at the ATJ and zero at the CTJ. Electric field strength in the dielectric in relation to the field in the vacuum is described as

$$E_{ins} = \eta E \quad \textbf{(7)}$$

where

$$\eta = \frac{\sin(\nu\theta)}{\sin(\nu\beta)}. \quad \textbf{(8)}$$

For the modeled 45° insulator case, η at the ATJ is 0.67858 and η at the CTJ is 1.47367.

Given this set of theoretical benchmarks, comparisons between the computed values and the modeled case were drawn. The accuracy of the "zooming" method and its use as an analysis tool for small details in a large solution space was also studied.

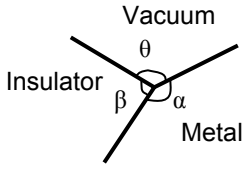

	ATJ	CTJ
Metal (α)	π	π
Insulator (β)	3π/4	π/4
Vacuum (θ)	π/4	3π/4

Figure 6. Definition of angles by Chung et al. and the corresponding values for the modeled geometry

IV. ANALYSIS

The theory noted in the previous section provides excellent groundwork for triple junction electrostatic model verification. The model described in Sec. II was evaluated at all stages of the zooming process. The most information about the validity of zoom was gleaned from the 0.2 μm mesh. The 30 μm mesh (global case) provided a useful demonstration of the assumptions or limitations used in the analytical model.

From the initial line scans described in Sec. II and shown in Figure 4 and Figure 5, it can be concluded that the shape of the curves is concurrent with Equation 5 and Equation 6. Assuming that the curves also agreed with Equation 1, the analysis of the model began with the calculation of ν. The output from the model included electric field values and the

corresponding coordinates. Stating Equation 1 in a different form,

$$\ln(E) = (\nu - 1)\ln(r) + \ln(C). \qquad \textbf{(9)}$$

The linearity of the plots in Figure 7 and Figure 8 can be exploited to determine ν values for both the ATJ and CTJ. The slopes of the ATJ scan line data in Figure 7 in the insulator and vacuum are -0.15328 and -0.15257 respectively. These values are remarkably similar to the theoretical value of -0.15222 stated in the previous section. The same holds true for the CTJ theoretical value of 0.15222. Slope values for the CTJ scan line data in Figure 8 in the insulator and the vacuum are 0.15270 and 0.15263 respectively.

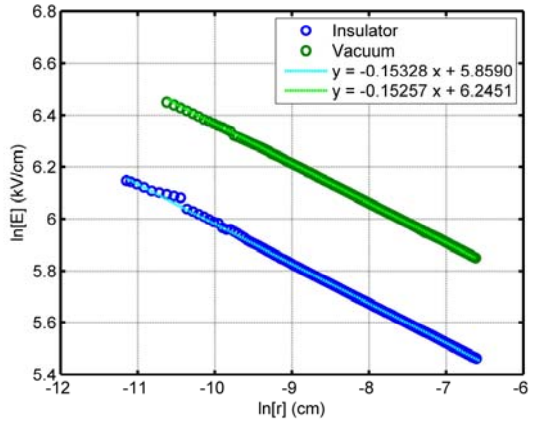

Figure 7. ATJ line scan data for 0.2 μm mesh

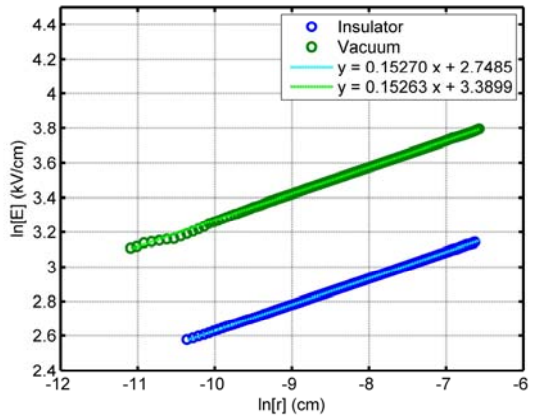

Figure 8. CTJ line scan data for 0.2 μm mesh

Another theoretical comparison can be drawn from the relationship between the line scan values in vacuum and in the insulator. Equation 7 and Equation 8 describe the relationship between the electric fields in vacuum and insulator. Applying the computed values from the previous section to the 0.2 μm data, the theoretical prediction of the electric field value in the insulator demonstrates excellent correlation to the scan line data. These results are seen in Figure 9 and Figure 10.

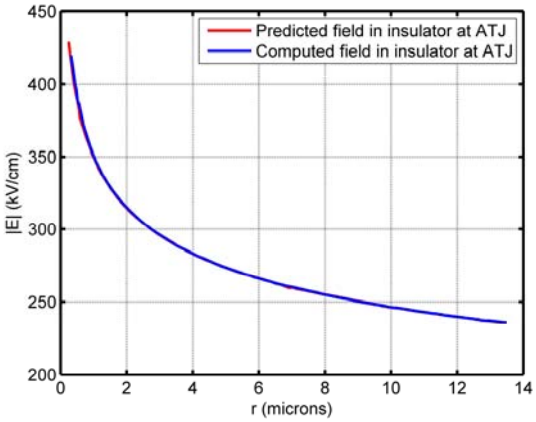

Figure 9. Predicted and computed values of electric field strength at ATJ

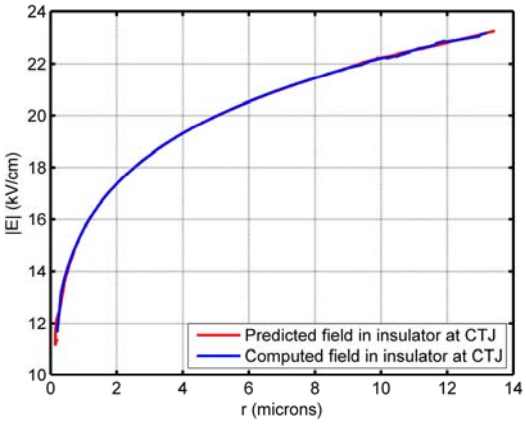

Figure 10. Predicted and computed values of electric field strength at CTJ

A final theoretical and computational comparison can be made from Equation 1. The values of r and ν are known or can be computed from the geometry. Electrostatic field modeling allows for the calculation of C. Using the theoretically calculated ν value and computationally calculated C value, a plot can be constructed to show the relationship between the fields obtained from software and the fields near the triple junctions obtained from a combination of software (C) and theory (ν). The relationship is plotted in Figure 11.

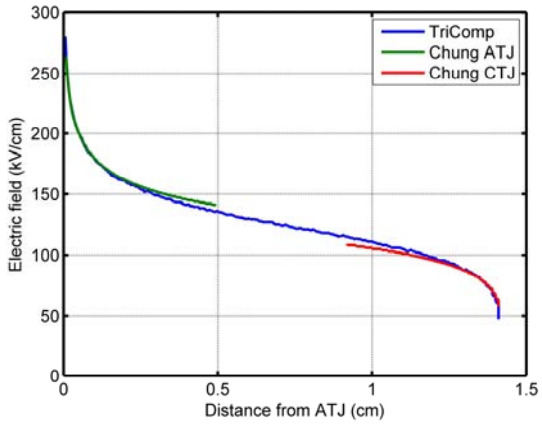

Figure 11. Relationship of computed fields to theoretical fields

V. SUMMARY

A baseline 45° degree insulator case was modeled using the TriComp software suite. The "zoom" feature was employed to study the anode and cathode triple junctions at a submicron level. Results from such models were compared to the analytical analysis provided by Chung et al. Good correlation between the analytical and computational methods was noted. In these studies, the iterative zooming achieved with this software appears to be a powerful modeling technique.

VI. ACKNOWLEDGEMENTS

This work was performed under the auspices of the U.S. Department of Energy by University of California, Lawrence Livermore National Laboratory under Contract W-7405-Eng-48. The project 06-ERD-033 was funded by the Laboratory Directed Research and Development Program. The authors would like to thank George Vogtlin and Gene Lauer for their helpful counsel and discussion on this project. Additional thanks to Andy Poggio for his review of this document.

VII. REFERENCES

[1] Field Precision LLC, PO Box 13595, Albuquerque, NM 87192. www.fieldp.com

[2] TriComp 5.0, EStat: Finite-element Electrostatics, Field Precision, 2002.

[3] T. Takuma, T. Kouno, and H. Matsuda, "Field behavior in composite dielectric arrangement", *IEEE Trans. Electr. Insul.*, vol. EI-13, no 6, pp. 426-435, Dec. 1978.

[4] T. Takuma, "Field behavior at a triple junction in composite dielectric arrangements", *IEEE Trans. Electr. Insul.*, vol. 26, no. 3, pp. 500-509, June 1991.

[5] M.S. Chung, B-G. Yoon, P.H. Cutler, and N.M. Miskovaky, "Theoretical analysis of the enhanced electric field at the triple junction", *J. Vac. Sci. Technol. B*, vol. 22, no. 3, pp. 1240-1243, May 2004.

[6] M.S. Chung, T.S. Choi, B-G. Yoon, "Theoretical analysis of the field enhancement in a two-dimensional triple junction", *Applied Surface Science*, vol. 251, no. 1-4, pp. 177-181, Sept. 2005.

[7] M.S. Chung, S.C. Hong, P.H. Cutler, N.M. Miskovsky, B.L. Weiss, A. Mayer, "Theoretical analysis of triple junction field emission for a type of cold cathode", *J. Vac. Sci. Technol. B*, vol. 24, no. 2, pp. 909-912, Mar. 2006.